Supporting Information

Confined deep red light-detecting organic phototransistors with polymer gate-sensing layers consisting of indacenothiophene and dinitrobenzothiadiazole units

Chanbin Park[a,b], Taehoon Kim[a], Hwajeong Kim[a,c] and Youngkyoo Kim[a,b*]

[a] Organic Nanoelectronics Laboratory and KNU Institute for Nanophotonics Applications (KINPA), Department of Chemical Engineering, School of Applied Chemical Engineering, Kyungpook National University, Daegu 41566, Republic of Korea

[b] Department of Energy Convergence & Climate Change and Institute for Global Climate Change and Energy, Kyungpook National University, Daegu 41566, Republic of Korea

[c] Priority Research Center, Research Institute of Environmental Science & Technology, Kyungpook National University, Daegu 41566, Republic of Korea

*Corresponding Author: Prof. Y. Kim

E-mail) ykimm@knu.ac.kr Tel) +82-(0)53-950-5616

Table S1. Summary of photoresponsivity (R_C) and photosensitivity (S_P) for the OPTRs with the GSLs and VLCLs under illumination. Note that the incident light intensity (P_{IN}) was 162, 277, and 281 $\mu W/cm^2$ at the wavelength (λ) of 550, 670, and 700 nm, respectively.

Wavelength (nm)	Thickness (nm)	S_P (%)		R_C (mA/W)	
		w/o VLCL	w/ VLCL	w/o VLCL	w/ VLCL
550	40	96.43	0.31	2.23	0
	120	92.17	0	1.53	0
670	40	43.25	30.64	0.58	0.41
	120	48.16	31.46	0.47	0.34
700	40	28.12	20.19	0.37	0.26
	120	32.28	30.14	0.32	0.31

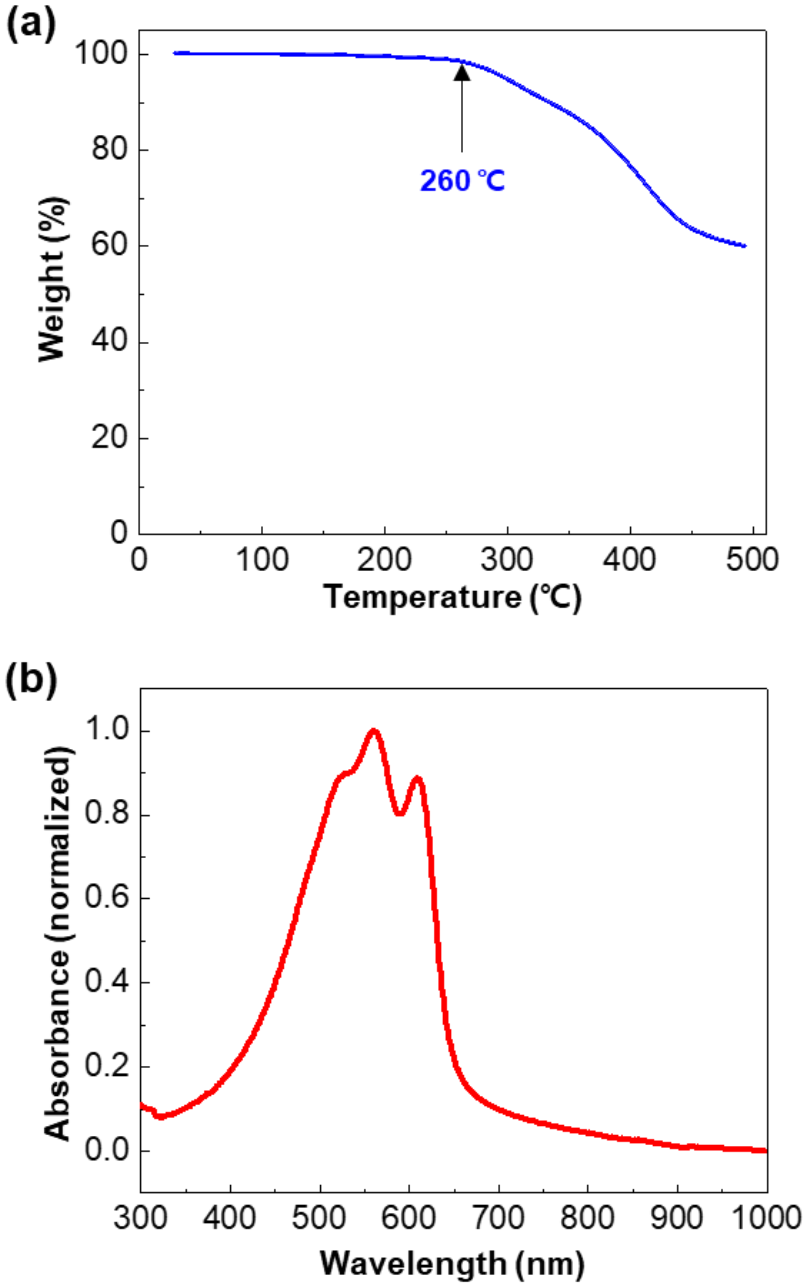

Figure S1. (a) TGA thermogram of PIDTT-DNBT solid (ramp rate = 10 ℃/min under nitrogen flow). (b) Optical absorption spectrum for the thin P3HT film (t = 80 nm).

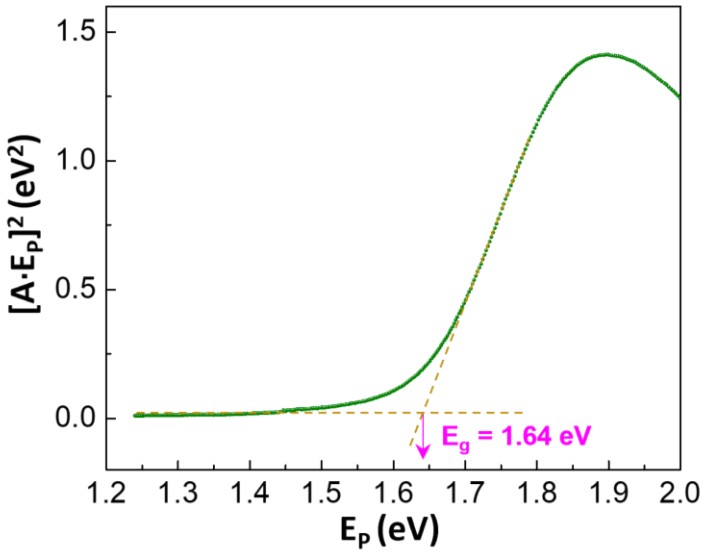

Figure S2. Tauc plot of the PIDTT-DNBT film from the optical absorption spectrum in Figure 1(b). 'A' and 'Ep' denote absorbance and photon energy, respectively.

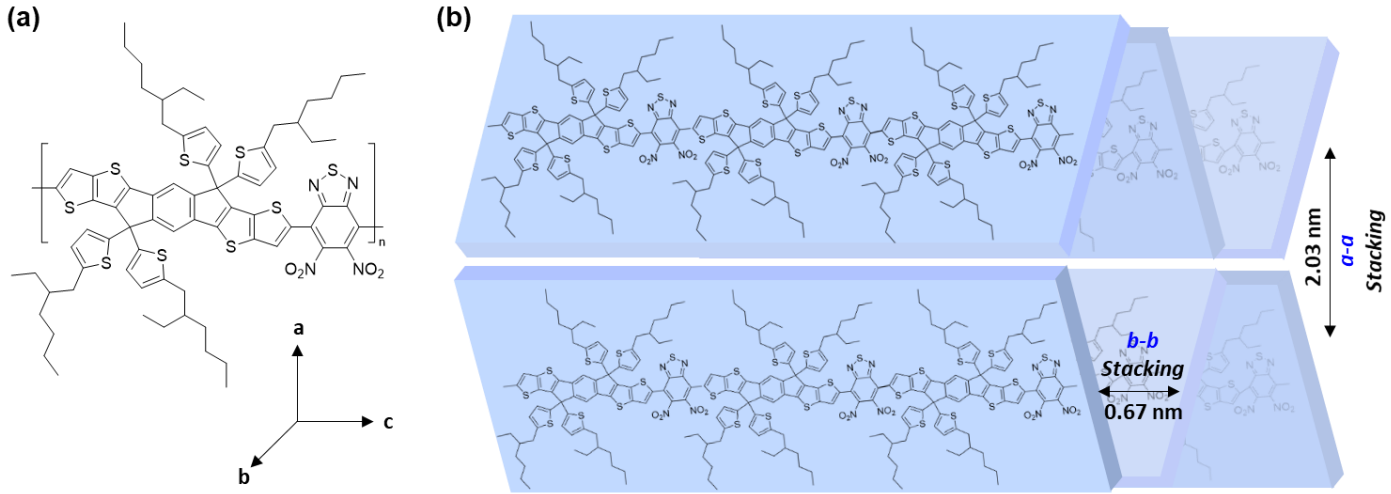

Figure S3. (a) Assignment of axis according to the molecular structure of PIDTT-DNBT. (b) Illustration for the possible stacking structure of PIDTT-DNBT chains. The stacking distance (d-spacing) in the a-a and b-b directions was calculated from the GIWAXS profiles.

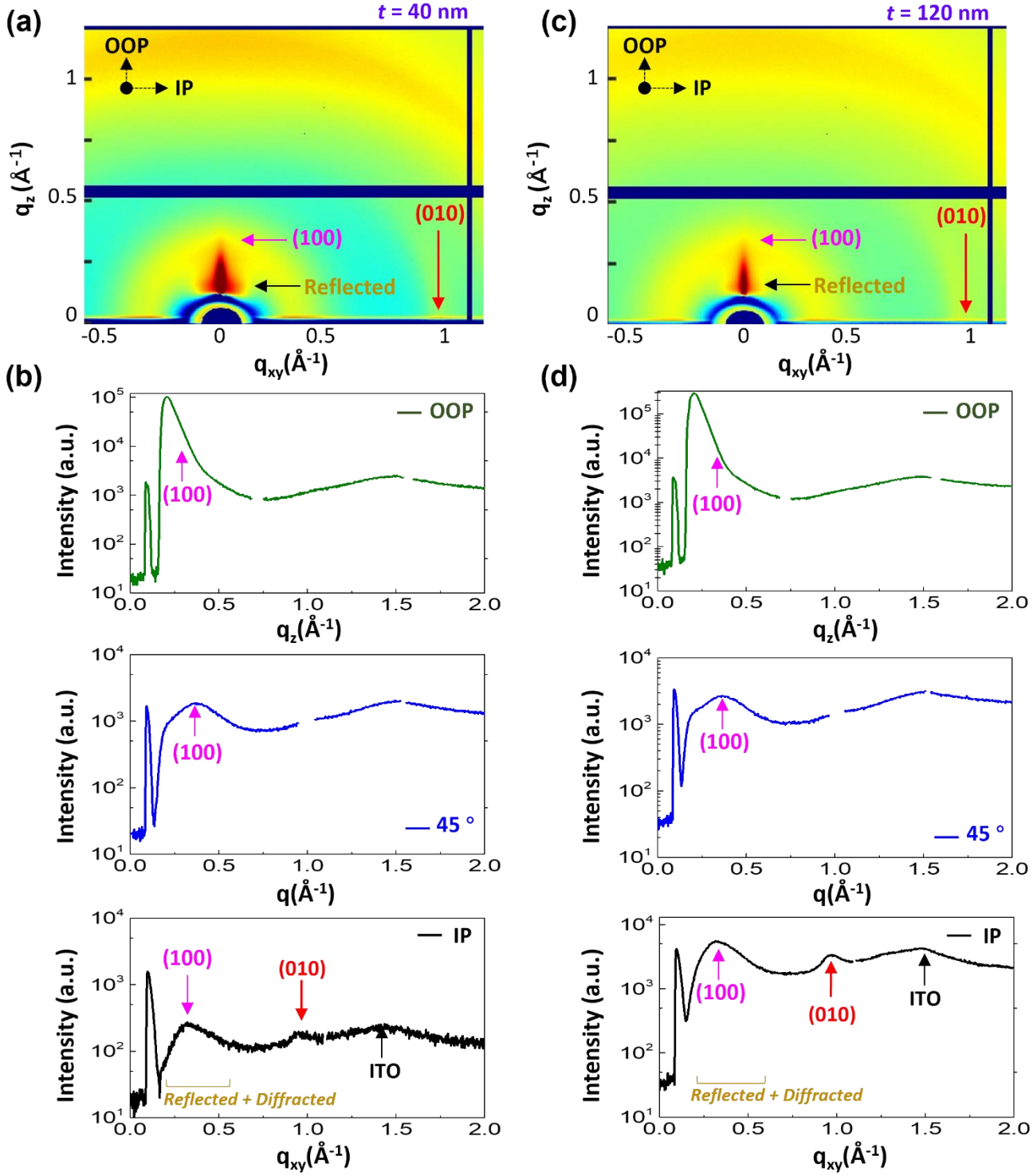

Figure S4. GIWAXS data for the PIDTT-DNBT films (t = 40 nm and 120 nm): (a,c) 2D images, (b,d) 1D profiles. OOP and IP denote the out-of-plane and in-plane directions in the films, respectively. Note that the 1D profile at 45° was obtained by extracting scattering data at the azimuthal angle of 45° in the 2D image (see Y. Kim et al., Soft Matt., 3, 117 (2007)).

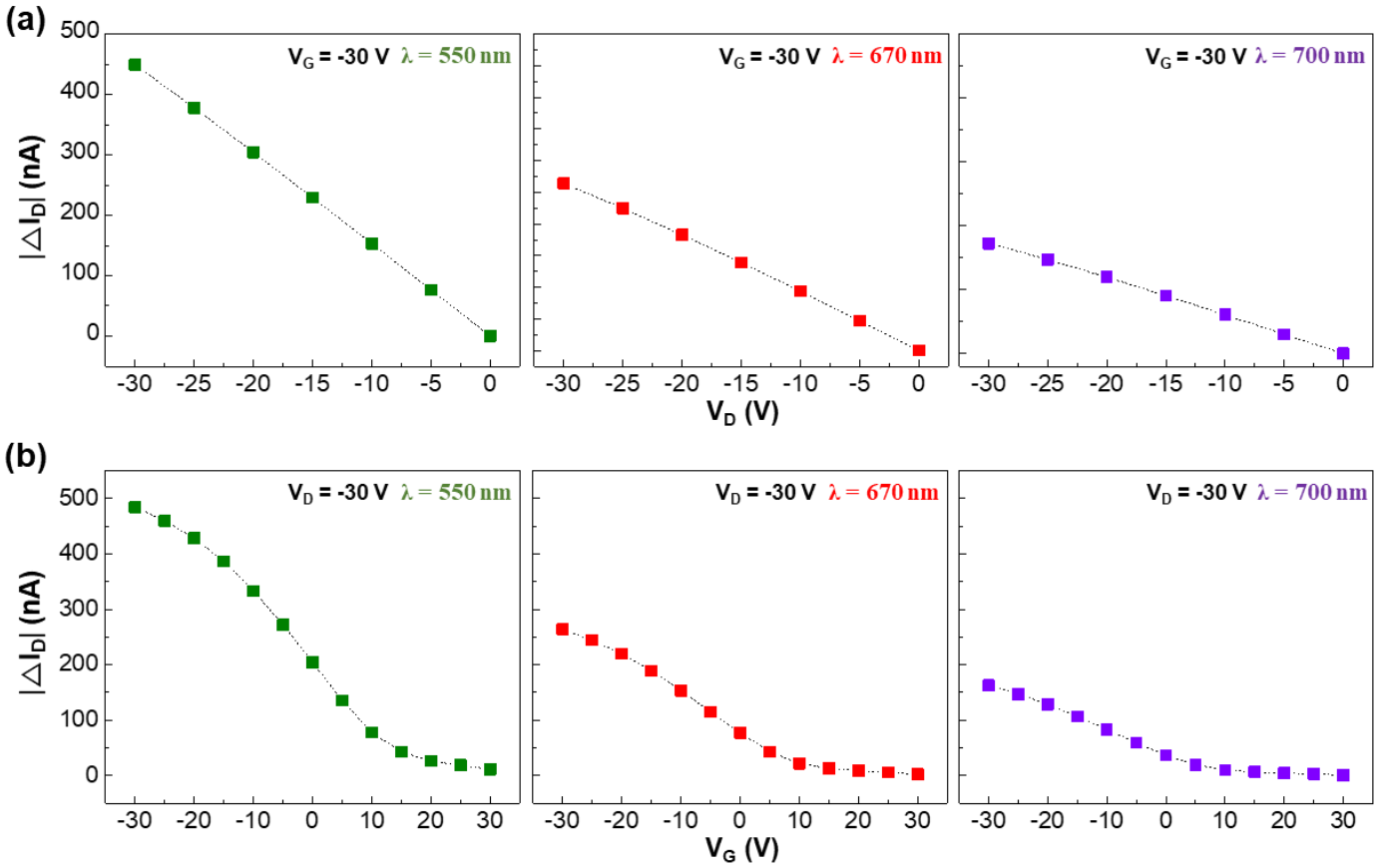

Figure S5. Net drain current ($\triangle I_D$) for the OPTRs with the PIDTT-DNBT GSLs (t = 40 nm) (no VLCLs) under illumination with three different monochromatic lights: (a) from output curves, (b) from transfer curves. Note that the incident light intensity (P_{IN}) was 162, 277, and 281 $\mu W/cm^2$ at the wavelength (λ) of 550, 670, and 700 nm, respectively.

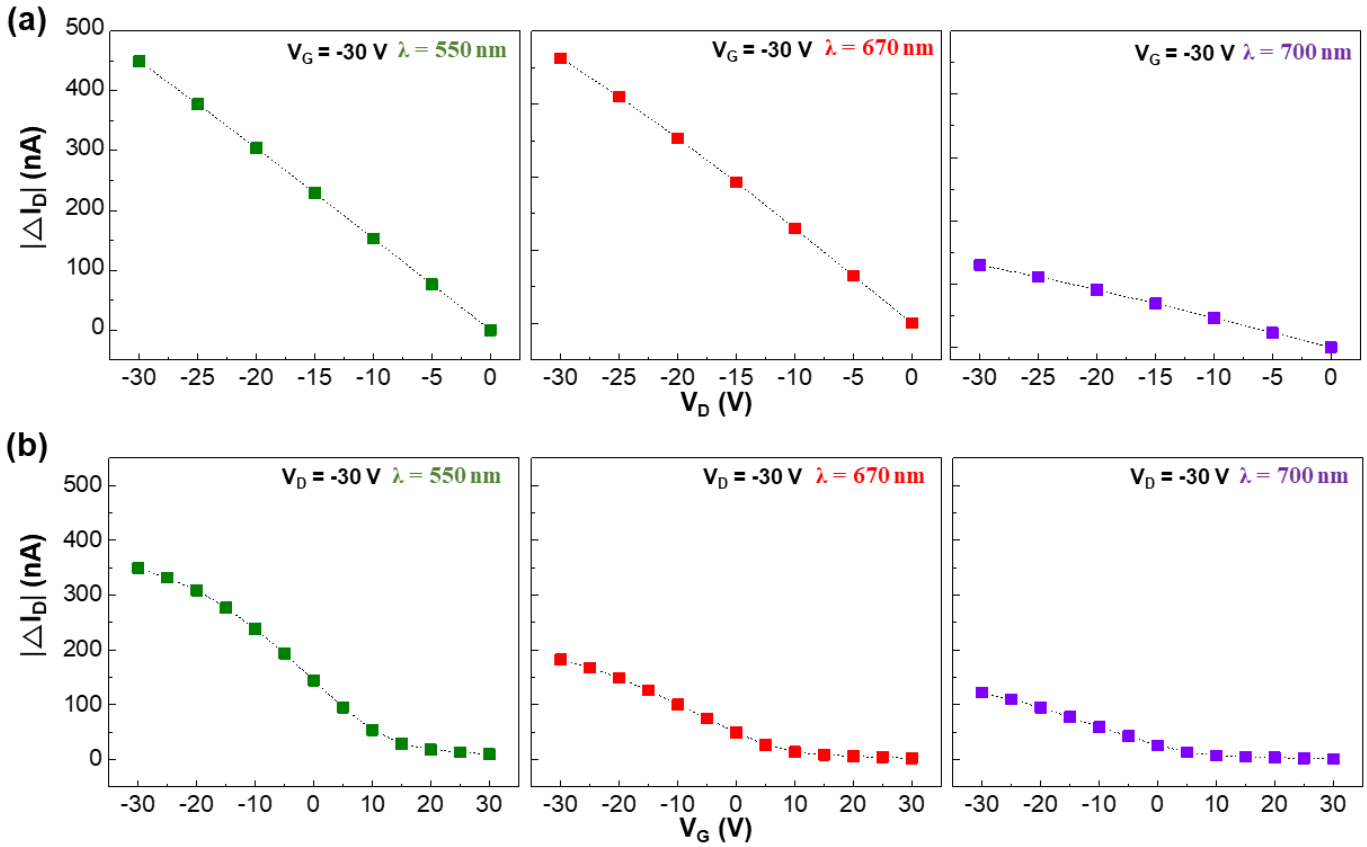

Figure S6. Net drain current (△I_D) for the OPTRs with the PIDTT-DNBT GSLs (t = 120 nm) (no VLCLs) under illumination with three different monochromatic lights: (a) from output curves, (b) from transfer curves. Note that the incident light intensity (P_{IN}) was 162, 277, and 281 $\mu W/cm^2$ at the wavelength (λ) of 550, 670, and 700 nm, respectively.

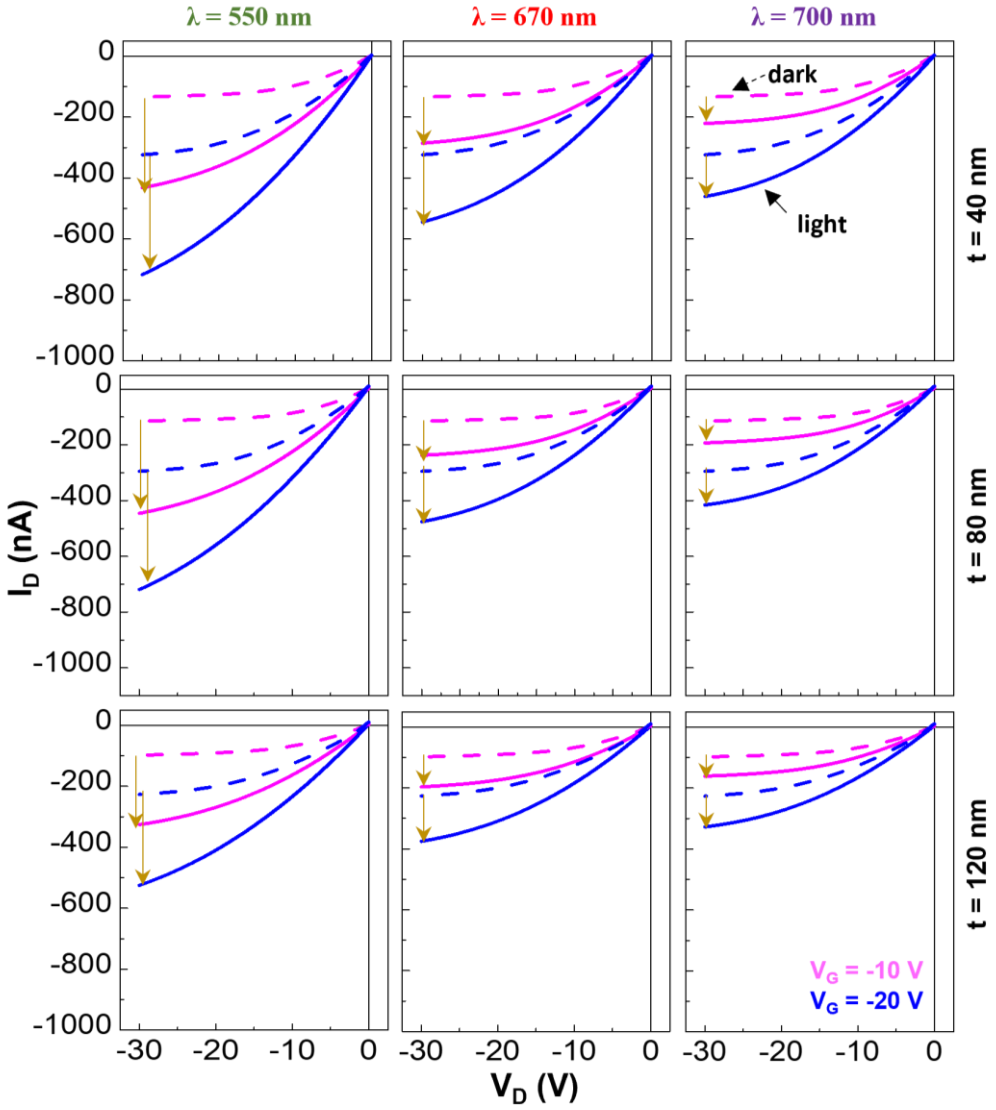

Figure S7. Change of drain current (V_G = -10 V and -20 V) in the output curves for the OPTRs with the PIDTT-DNBT GSLs (t = 40, 80, 120 nm) (no VLCLs) under illumination with three different monochromatic lights. Note that the incident light intensity (P_{IN}) was 162, 277, and 281 $\mu W/cm^2$ at the wavelength (λ) of 550, 670, and 700 nm, respectively.

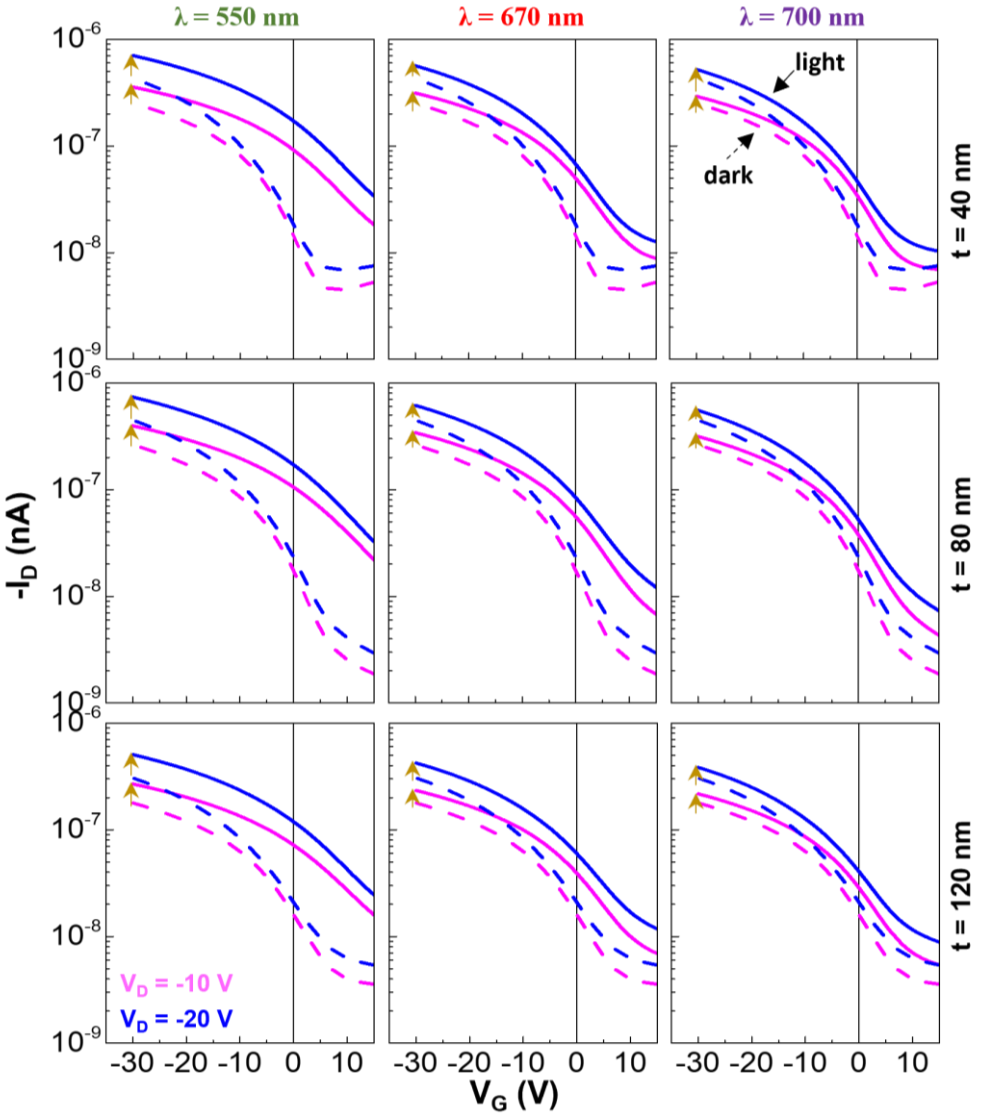

Figure S8. Change of drain current (V_D = -10 V and -20 V) in the transfer curves for the OPTRs with the PIDTT-DNBT GSLs (t = 40, 80, 120 nm) (no VLCLs) under illumination with three different monochromatic lights. Note that the incident light intensity (P_{IN}) was 162, 277, and 281 $\mu W/cm^2$ at the wavelength (λ) of 550, 670, and 700 nm, respectively.

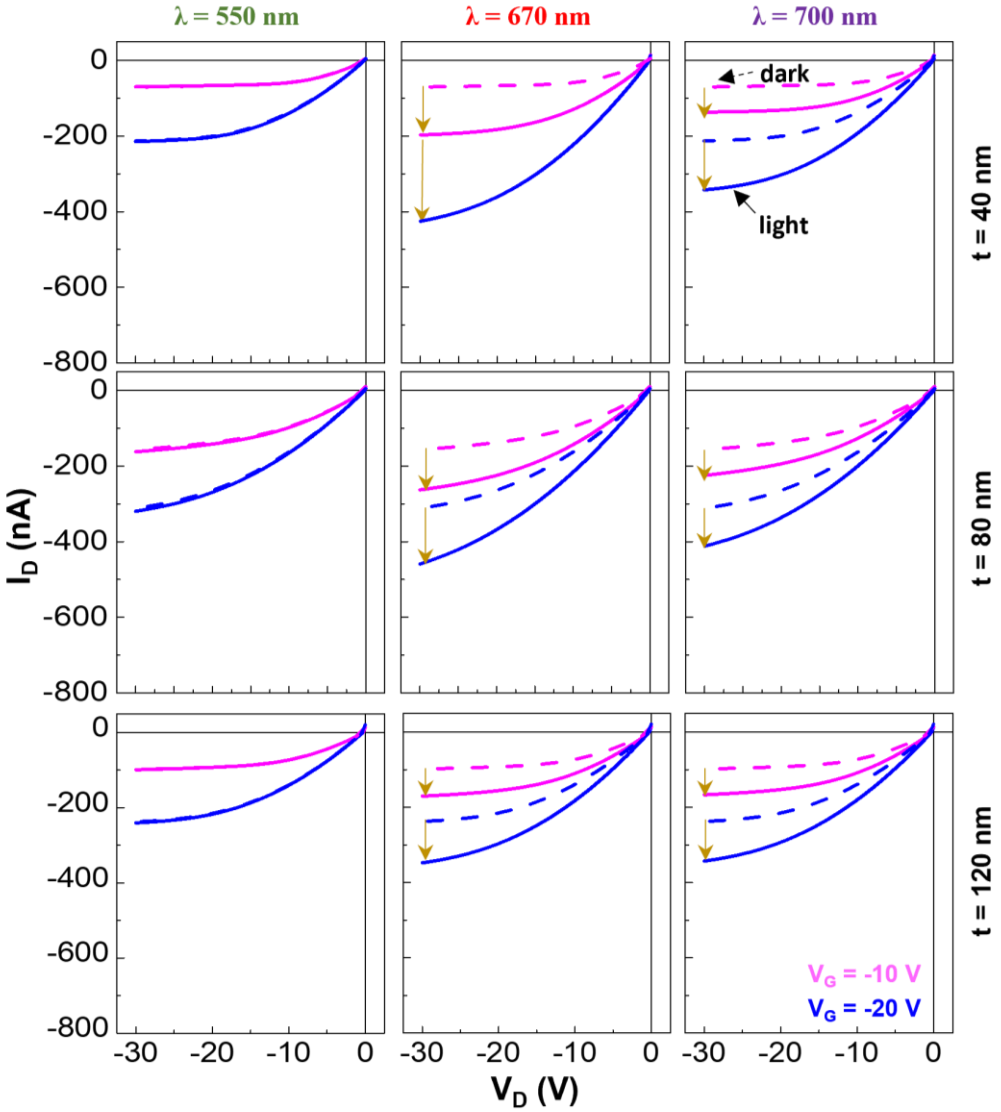

Figure S9. Change of drain current (V_G = -10 V and -20 V) in the output curves for the OPTRs with both the PIDTT-DNBT GSLs (t = 40, 80, 120 nm) and the VLCLs under illumination with three different monochromatic lights. Note that the incident light intensity (P_{IN}) was 162, 277, and 281 $\mu W/cm^2$ at the wavelength (λ) of 550, 670, and 700 nm, respectively.

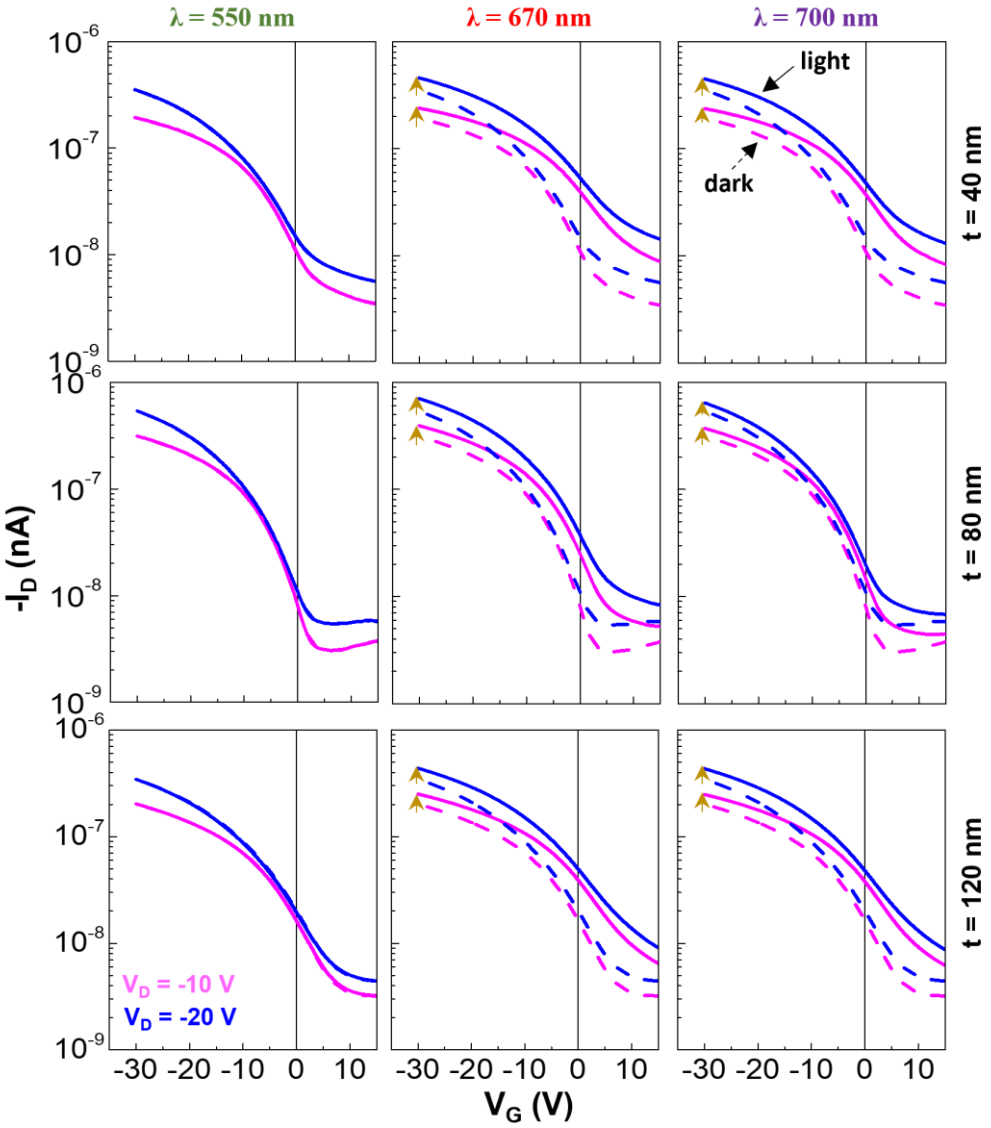

Figure S10. Change of drain current (V_D = -10 V and -20 V) in the transfer curves for the OPTRs with both the PIDTT-DNBT GSLs (t = 40, 80, 120 nm) and the VLCLs under illumination with three different monochromatic lights. Note that the incident light intensity (P_{IN}) was 162, 277, and 281 $\mu W/cm^2$ at the wavelength (λ) of 550, 670, and 700 nm, respectively.

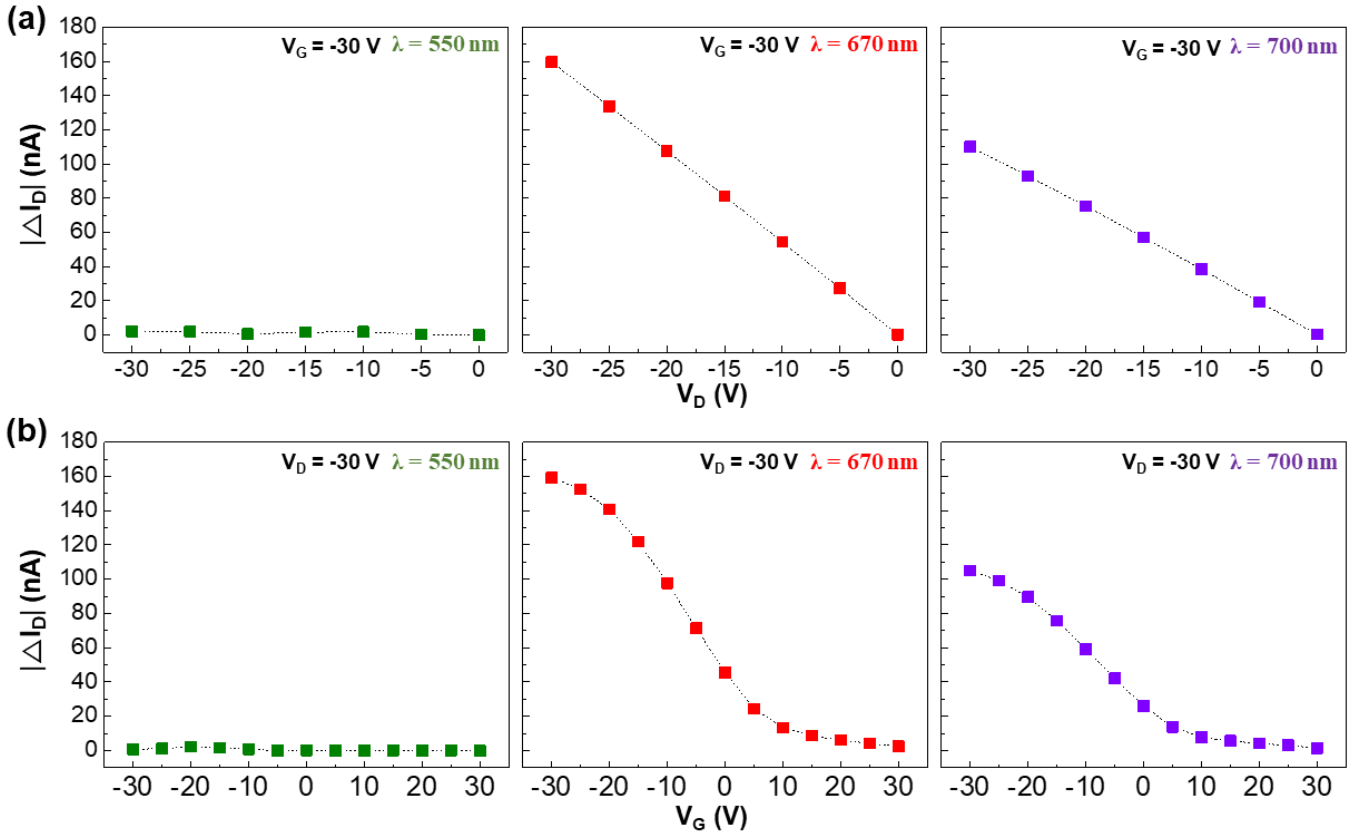

Figure S11. Change of net drain current (ΔI_D) for the OPTRs with both the PIDTT-DNBT GSLs (t = 40 nm) and the VLCLs under illumination with three different monochromatic lights: (a) from output curves, (b) from transfer curves. Note that the incident light intensity (P_{IN}) was 162, 277, and 281 $\mu W/cm^2$ at the wavelength (λ) of 550, 670, and 700 nm, respectively.

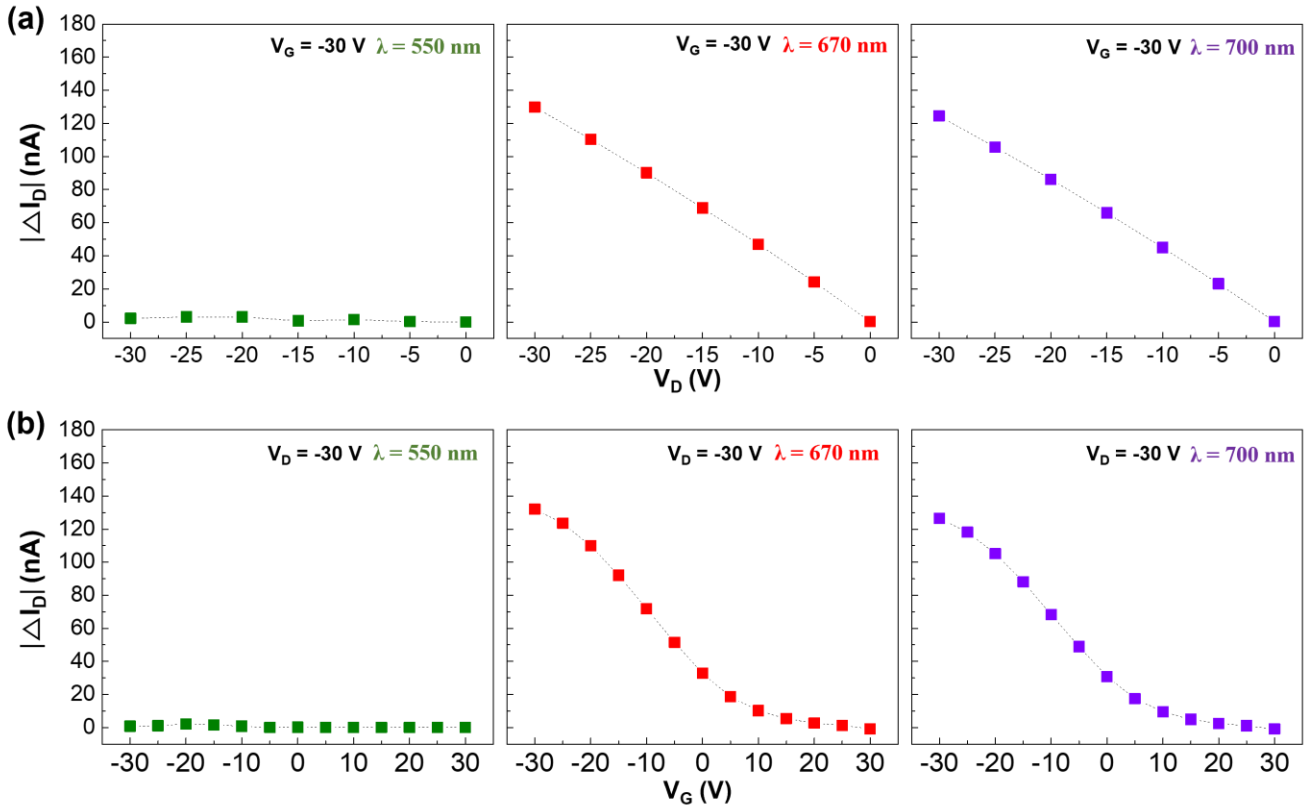

Figure S12. Change of net drain current ($\triangle I_D$) for the OPTRs with both the PIDTT-DNBT GSLs (t = 120 nm) and the VLCLs under illumination with three different monochromatic lights: (a) from output curves, (b) from transfer curves. Note that the incident light intensity (P_{IN}) was 162, 277, and 281 $\mu W/cm^2$ at the wavelength (λ) of 550, 670, and 700 nm, respectively.